Shear crack width assessment in concrete structures by 2D distributed optical fiber

Gerardo Rodriguez[1], Joan R. Casas[2] & Sergi Villalba[3]

[1]*Institute of Engineering, National Autonomous University of Mexico UNAM. Mexico City, Mexico*

[2]*Technical University of Catalonia, UPC-BarcelonaTech. Department of Civil and Environmental Engineering, Barcelona, Spain*

[3]*Technical University of Catalonia, UPC-BarcelonaTech. Department of Project and Construction, Terrassa, Spain*

Corresponding author: Tel.: +556233600 ext. 8417 email: grog@pumas.ii.unam.mx

Abstract. This paper outlines the second part of an experimental study to show the capabilities of distributed optical fiber sensors (DOFS) in their application to the structural health monitoring (SHM) of the shear performance of concrete structures. SHM seeks to obtain the shear crack characteristics of concrete elements: detection, localization and quantification of shear damage. The two first were discussed in the first part of the experimental study. In the present paper, the quantification is dealt with by proposing a method to obtain the mean shear crack width in concrete beams. The method is based on the experimental data obtained by a DOFS bonded to the concrete surface. First, the basis of the methodology are presented and, later on, experimentally checked by testing of three partially pre-stressed concrete (PPC) beams subjected to a shear test with increasing level of load. The DOFS were deployed in the web of the beams to conform a 2D grid mesh to measure the strain profile along two orthogonal directions. The experimental data was obtained using an OBR (Optical Backscattered Reflectometer) system with high spatial resolution and sensitivity that allow a complete mapping of the cracking pattern and to obtain the required data for the calculation of the crack width. The results show the feasibility of the proposed method in calculating the shear crack width when compared to the results from traditional instrumentation.

Keywords: shear crack width, Distributed Optical Fiber Sensors (DOFS), Rayleigh backscatter, Optical Backscattered Reflectometer (OBR)

1. Introduction

One of the most important parameters to quantify the level of damage in a concrete structure is the presence of cracks. Cracking behaviour and control of crack width are significant factors in the design of concrete structural members. Nowadays, most formulations to evaluate and control the crack width have been originally developed for tensile and flexural cracks. In the specific case of shear stresses, there is not a specific methodology to evaluate the shear crack width in concrete members [1]. This is because the mechanism of diagonal cracking is not perpendicular to the vertical reinforcement and it is more complex than axial or bending cracking [2]. The few methodologies to evaluate shear cracks width in concrete members are based on several experimental and analytical studies [1, 3, 4]. However to obtain experimental data in these formulations during and after the test, several manual and observational activities have to be performed such as tracing the crack pattern with a marking pen, or measuring the cracks width progression by using visual techniques. It is important to consider the implications, since several measuring errors could appear in all of these activities. In this paper, a method to obtain the mean shear crack width in concrete structures using experimental data obtained with distributed optical fiber sensor (DOFS) connected to an optical backscattered reflectometer (OBR) system is proposed. Nowadays, similar DOFS techniques are applied to study several engineering problems [5,6,7]. In the specific cases of early crack detection the OBR systems have demonstrated their effectiveness, both for embedded optical fiber cables [8,9,10] and for optical fiber cables bonded to the surface of concrete structures, either with a thick external coating protection [9,10] or directly bonded [11,12,13]. The main characteristics of this methodology are the use of an optical fiber

attached to the concrete surface. In the specific case of shear cracks, as presented in this paper, the proposal is to bond a 2D mesh to the surface of the beams to measure the strain profiles along 2 orthogonal directions. Thanks to the high spatial resolution and sensitivity of the OBR system, the strain variation registered is practically continuous and cracks can be detected, located and quantified.

2. OBR Method for shear crack width assessment in concrete structures

Theoretical background

The experimental configuration of the OBR methodology based on Rayleigh backscatter to obtain the shear cracking pattern in concrete structures is divided in the test set-up and the theoretical bases. A complete description of the test set-up is described later in section 5 of this paper and is fully available in [14]. In this section, the theoretical background of this methodology is developed. An arrangement with one or two DOFS is proposed to form a grid within the area in which these cracks are expected to occur (zone of maximum shear within the element). A schematic representation is shown in Fig 1. The strain profiles in two orthogonal directions will serve to obtain the inclination of the crack and the crack width.
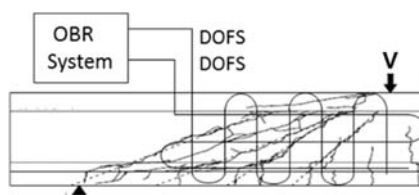

Fig.1. Rectangular 2D mesh formed by the DOFS for the characterization of shear cracking.

In this research, the authors used a polyimide coated fiber that had a combined total diameter of core, cladding and coating of 155 μm, being that the coating only contributed with 15 μm for this diameter with the objective to protect the fiber against scratches and environemental attack, but reducing the influence of the sensor coating material in the strain accuracy of the DOFS measurements. Therefore, the The DOFS used was a silica (glass) single-mode fiber with a core diameter of 2 mm and a thin coating of a polymer (polyimide) to protect the fiber against scratches and environmental attack. The DOFS used in this study is a practically nude fiber able to transfer any strain or temperature variation form the host material to the fiber core without any other material in between. In this way, the analysis of the experimental results isare much simpler, with the disadvantage of a lower ess protection when compared to other DOFS. ed sensor. However, tThis is not an issue in the case of tests in the laboratory, , where much care is taken than in real world structures. and the same type of fiber was used However, OBR system also applied by the authors with success this deployment methodology in some real structures [16]. Firstly, to carry out the localization of the cracks and the identification of the shear cracking pattern in the concrete element, a coordinate system X-Y was defined. A set of coordinates (x_n, y_n) is assigned to all the points that conform the rectangular mesh defined by the DOFS. Subsequently, horizontal (identified with letters) and vertical (identified with numbers) stretches are defined, and different sections are established within this mesh, as seen in Fig. 2a. From here, when static load is incrementally applied gradually with loading and unloading cycles, the strain profile in two perpendicular directions is obtained at the zone of interest. In Fig.2b, the evolution of the strain with the load (time) in some points in the horizontal direction is presented. In these points, there is no cracking during the test and, therefore, they perfectly follow a sequence along time similar to the loading (see Fig. 10). However, it is evident an increase in the strain level as the monitored points become closer to the shear crack.

Through the coordinates (x_n, y_n), any measuring DOFS point is identified. These coordinates are a function of the spatial resolution assigned in the OBR system, which in this case was of 1 cm. In the case of the 2D mesh, the spatial resolution is translated into the increment Δx and Δy between the coordinates x_n, y_n in both directions, as indicated in Fig. 2. Afterwards and through the analysis

of the information obtained with the OBR system, the tracing of progressive cracking pattern in the instrumented area can be achieved. The strain variation along the fiber allows to identify the moment when cracking starts and its evolution through the loading process. A complete description of the methodology is available in [11,14]. The shear crack width assessment is based on the integration of strain data obtained with the OBR system. One example of this "quasi" continuous data (obtained with a space resolution of 1 cm) along the horizontal x-direction is shown in Fig. 3. The horizontal line in Fig. 3 corresponds to the maximum tensile strain of the concrete (ε_{fctx}). When this threshold value is exceeded, the peaks associated with the presence of cracks appear.
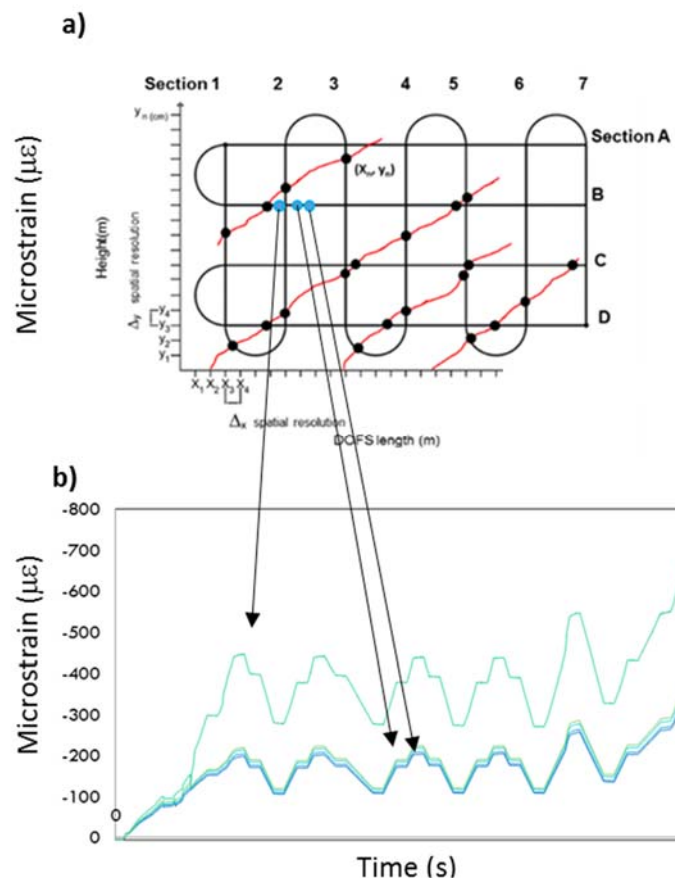

Fig.2. 2D mesh conformed by DOFS to obtain the shear cracking pattern.
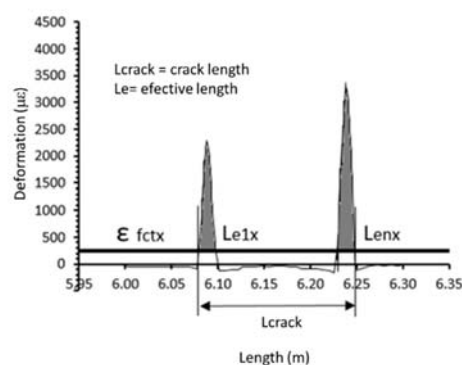

Fig. 3. Example of OBR shear strain data.

One of the characteristics of the OBR records in a shear test is that the concrete surface presents tension values only in the cracks, and due to the shear stress mechanism concrete between cracks is mainly in compression as also shown in Fig 3. In this figure, a characteristic length of cracked concrete (L_{crack}) is considered. L_{crack} includes the entire area in which shear cracking occurs. Additionally, in each direction x or y, one or more effective lengths called L_{enx} or L_{eny} are defined

(Fig. 4). These lengths only include the zone in which the tensile strain of the concrete ε_{fctx} or ε_{fcty} is exceeded in each direction x or y. The trace of the shear cracking pattern is carried out as described in Fig. 4. In the 2D mesh formed by the DOFS, one or more cracks are detected simultaneously in two orthogonal directions X and Y for a given value of the test load. Generally, as mentioned, in the horizontal direction most of the concrete is in compression except those points where cracks have been detected. These records associated with the X direction are identified by a letter, starting with the A and in descending order with respect to the height of the beam (see Fig. 4). To define the integration area under the curve in a given DOFS horizontal section and apply the OBR method for calculating the shear crack width, the strain associated with the maximum concrete tension in direction x is obtained as $\varepsilon_{fctx} = \varepsilon_{fct} * \sin\theta$, where ε_{fct} is the maximum tensile strain of concrete and θ is the angle of the shear crack at that point. The same process is carried out in each of the monitored horizontal sections. Initially, the angle θ is unknown, but, it can also be obtained thanks to the data coming from the DOFS as described later. In this way, equation 1 can be established for the DOFS in direction X. The right side of equation 1 represents the mean strain in the cracked zone in direction X as the integral of the strain in each of the n effective lengths (L_{eix}) where a crack is present.

$$\varepsilon_{mean\,x} = \frac{1}{L_{e\,total\,x}} \sum_{i=1}^{n} \int_{0}^{L_{eix}} \varepsilon_{OBRix}\,dx \qquad (1)$$

Where:

$$L_{e\,total\,x} = \sum_{i=1}^{n} L_{eix}$$

A similar process is carried out with the vertical strain data. In the vertical records, the assignment of the cracked length (L_{cracky}) is carried out as in the case of bending [11] as shown in Fig. 4. This is based on the fact that in the vertical direction, tension usually appears at various points. . The Y direction of the reference system is associated to the different DOFS vertical sections, and for their identification, a number starting with 1 is assigned (Fig. 4). Similarly to the X direction, in the Y direction, the threshold value from which the integration of the OBR record is performed is the maximum tensile strain in vertical direction: $\varepsilon_{fcty} = \varepsilon_{fct} * \cos\theta$. Again, the mean strain in Y direction can be established using equation 2.

$$\varepsilon_{mean\,y} = \frac{1}{L_{e\,total\,y}} \sum_{i=1}^{n} \int_{0}^{L_{eiy}} \varepsilon_{OBRiy}\,dy \qquad (2)$$
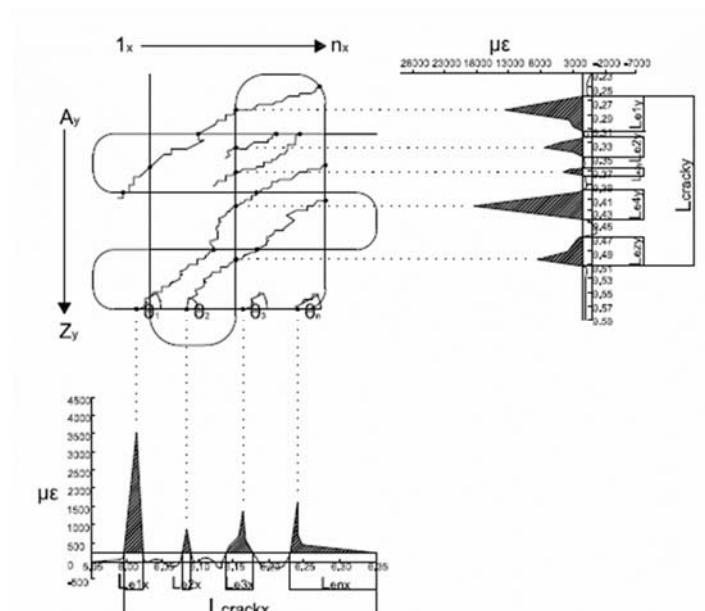
Where:

Fig. 4. Procedure for locating, tracing and calculating shear crack widths.

On other hand, the mean strain (ε_{mean}), in both X and Y directions, can also be obtained from equations 3 and 4.

$$\varepsilon_{meanx} = \varepsilon_{fctx} + \frac{\sum wx}{L_{crackx}} \qquad (3)$$

$$\varepsilon_{meany} = \varepsilon_{fcty} + \frac{\sum wy}{L_{cracky}} \qquad (4)$$

Then, equating equations (1) and (2) with equations (3) and (4), the value of the summation $\sum w$ can be obtained

$$\frac{1}{L_{e\,total\,x}} \sum_{i=1}^{n} \int_{0}^{Lei\,x} \varepsilon_{OBRi\,x}\,dx = \varepsilon_{fctx} + \frac{\sum wx}{L_{crack\,x}} \qquad (5)$$

$$\frac{1}{L_{e\,total\,y}} \sum_{i=1}^{n} \int_{0}^{Lei\,y} \varepsilon_{OBRi\,y}\,dy = \varepsilon_{fcty} + \frac{\sum wy}{L_{crack\,y}} \qquad (6)$$

In equations 5 and 6, $\sum wx$ and $\sum wy$ comprises the sum of the widths of all cracks w_x or w_y that occur within the cracked length. In this way, an average crack width is obtained in each direction x, y:

$$w_{mean\,x\,or\,y} = \frac{\sum w_{\,x\,or\,y}}{n} \qquad (7)$$

In equation 7 n is the number of cracks and is obtained by counting the peaks that occur in the continuous strain profiles of the OBR experimental results.
Finally, the average crack width is obtained through equation (8):

$$w_{mean} = \sqrt{w_{mean\,x}^2 + w_{mean\,y}^2} \qquad (8)$$

3. Experimental validation
Test set up
To evaluate and verify the method proposed in the previous section to monitor the crack width in concrete elements subject to shear, three partially pre-stressed concrete beams with 8 m span-length denominated I-1, I-2 and I-3 were tested. A three-point load test with the point load applied at a distance of 2 m from one of the supports of each beam were carried out as shown schematically in Fig 5. The test is designed to produce the shear failure of the beam. The cross-section, dimensions and arrangement of the transversal and longitudinal reinforcing steel and post-tensioning tendon are presented from Figs. 6 to 8 and in Table 1.
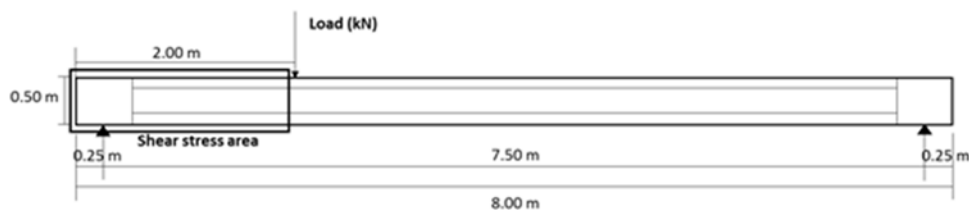

Fig. 5. Shear test set up of beam I-1, I-2 and I-3

The main differences in the beams are the amount of prestressing steel, shear reinforcement and web thickness. The diameter of stirrups is the same (6 mm) but with different spacing (Table 1). In Table 1, σp is the steel stress at jacking. The beams are post-tensioned by different number of strands within the duct.
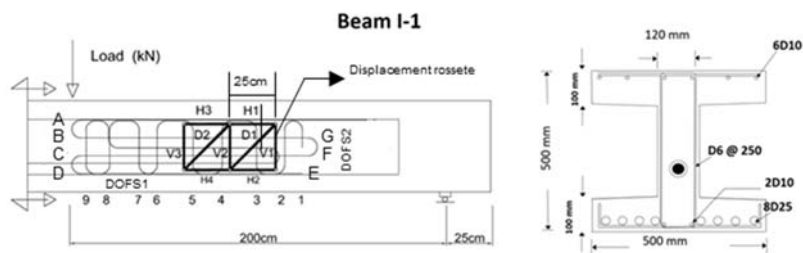
Beam I-1

Fig. 6. DOFS and displacement rosette to shear test of beam I-1.
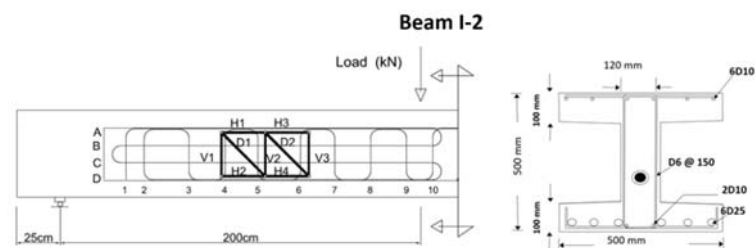
Beam I-2

Fig. 7. DOFS and displacement rosette to shear test of beam I-2.
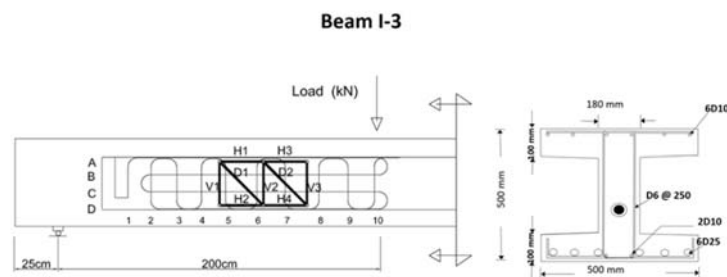
Beam I-3

Fig. 8. DOFS and displacement rosette to shear test of beam I-3.

To measure and compare experimentally the different crack widths, DOFS 2D mesh and displacements rosettes as shown in figures 6 to 8 were placed in the web of each beam. In the three tested beams the displacements rossettes are conformed by two quadrilateral arrangements with 25 cm of length as shown in Fig. 6. The DOFS 2D grids were conformed in the web of the beam with a DOFS1 of 10 m in horizontal direction and another DOFS2 of 5 m in length in the vertical direction, only in the case of beam I-1 (Fig. 6). , In the two remaining beams I-2 and I-3, the 2D grid was formed only with one DOFS of 10 m in length.

Table 1. Main characteristics of the beams

Beam	web thickness (mm)	Reinforcing steel		Prestressing steel			Stirrups spacing (mm)
		Upper	Botom	Strands	area (mm^2)	σp (Mpa)	
I-1	120	6 D10	8 D25+2 D10	2	300	1312	250
I-2	120	6 D10	6 D25+2 D10	2	300	1312	150
I-3	180	6 D10	6 D25+2 D10	4	600	1303	250

The horizontal grid sections were nominated with capital letters. The vertical sections were labeled using the numbers 1 to 10. Also from Figs. 6 to 8 each of the potentiometers that conform the displacement rosettes are identified. V1, V2 and V3 are vertical potentiometers, the upper horizontals H1 and H3, the lower horizontals H2 and H4, and the diagonals D1 and D2. The separation between the vertical potentiometers was approximately 25 cm, which involved covering a region of the web beams of approximately 50 cm (Figs. 6 to 8). The mechanical properties of the concrete are presented in Table 2, where f_{cm} is the mean concrete compressive strength, f_{ct} is the concrete tensile strength and E is the concrete elasticity modulus. The values of ε_{fct} are the maximum tensile concrete strain. All these values were obtained by the testing of the specimens moulded during the pouring of the beams and tested after 28 days.

Table 2. Concrete mechanical properties

Specimen	f_{cm} (Mpa)	f_{ct} (Mpa)	E (Mpa)	ε_{fct} με
I-1	32.5	4.6	36440	126
I-2	29.4	4.15	27264	152
I-3	41.5	5.86	34261	171

Based on the previous experiences by the authors in deploying DOFS in concrete structures, and a basic guidance on the bonding of these sensors established by the supplier [15] a bonding DOFS protocol was followed. This protocol is described in detail in [11, 12 13, 14]. The DOFS used was a single-mode fiber with a coating of a polymer (polyimide) to protect the fiber against scratches and environmental attack. Firstly, bond areas were cleaned and free from grease. A commercial glue was applied to the bond area (on the delimited shear zone of the web of each tested beam), avoiding to apply adhesive in excess. The glue used was an epoxy because some experiences [13, 16, 17, 18] have shown that in the laboratory environment, the installation with epoxy produces better results than using cyanoacrylate adhesives in concrete surfaces. According to that, a commercial bicomponent epoxy adhesive (Araldit) was applied to the bond area. The adhesive was applied to one of the bond surfaces, avoiding the use of tissue or a brush to spread the adhesive. As an example, Fig. 9 shows the final aspect of the DOFS 2D mesh and displacements rosettes arrangements in the web of the beam I-2 [14]. The radius of curvature in the curved parts of the fibers was approximately 8 cm, which is higher than the minimum diameter that has been used in previous studies, where this type of DOFS was deployed forming loops with radius of curvature as low as 1.27 cm with acceptable results [19].

To enhance durability and long-term performance of the fibers, in some cases, the sensing cable is protected with a thick external coating and attached to the surface with adhesive layers. In this case, strain profiles measured in the optical fiber may differ from actual strain in the substrate material. A posterior analysis is then necessary to obtain reliable measurements. Several mechanical tests, pull out tests and FEM numerical modelling had been developed to validate different methodologies to evaluate these effects [9, 10, 20]. However, in the present work, the fiber is stuck directly at the surface of concrete using an epoxy adhesive, what gives directly the changes in the substrate. In fact, a major issue with this configuration would be the durability of this sensing procedure when deployed in real structures and the possibility of a long-term monitoring. This will depend on the fact that the concrete itself could provide additional protection to the fiber, by

4. Test execution

The three beams I-1, I-2 and I-3 were tested under static load, applied gradually and with six loading and unloading cycles. The applied force was controlled by displacement of 1 and 2 mm / min, until the beams failed. The loading sequence is shown in Fig. 10. In this figure the total history of loading is indicated with a dash line. The DOFS break point is shown with a point and a continuous line. It is important to notice that from a certain level of load (indicated with a point and a thick continuous line), the results of the DOFS were not considered reliable because alternative strain changes from tension to compression were observed in the previous crack points identified. This behavior is associated to an incorrect performance of the sensor and to a SSQ (Spectral Shift Quality) values lower than 0.15, where, according to the manufacturer of the OBR system, the recorded values cannot be considered as accurate. Therefore, detection and location of shear cracks is limited to load levels around 262, 260 and 258 kN for the beams I-1, I-2 and I-3 respectively. In any case, these load levels produce high cracking and large deflections and therefore are far beyond the normal service load levels expected in real structures. A view of the experimental test setup is shown in Fig. 11. A complete and detailed description of the test results is available in [14].
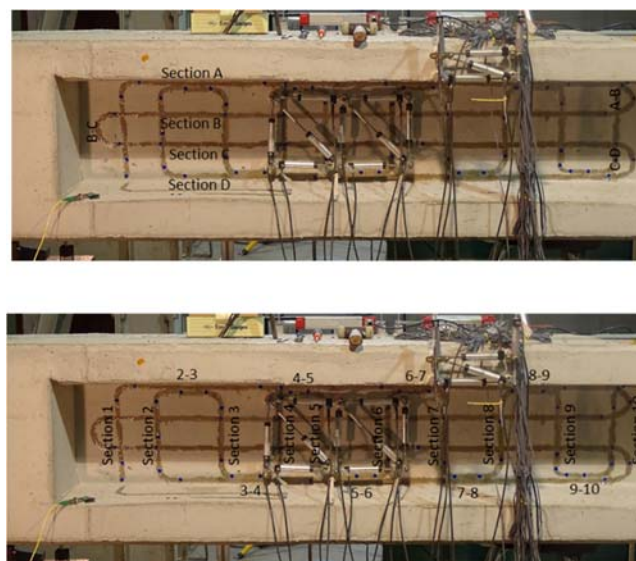

Fig. 9. DOFS 2D mesh and rosettes arrangements in the web of the beam I-2.
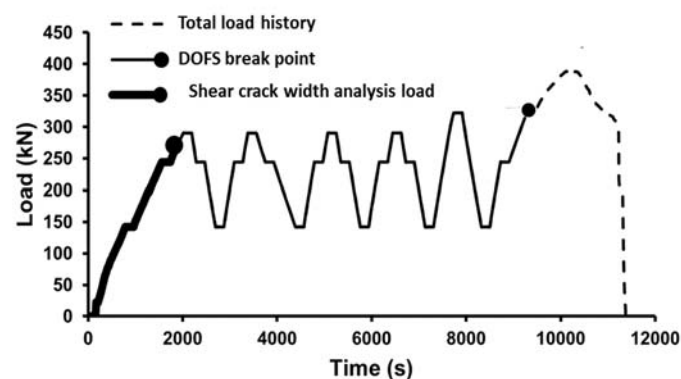
Fig. 10. Total loading sequence and part monitored with the DOFS 2D mesh in the tests

Fig. 11 Global view of experimental test of beam I-1 (Rodriguez et al 2016).

5 .OBR Measurement technique

OBR system uses swept-wavelength coherent interferometry to measure the Rayleigh backscattered as a function of position in the optical fiber. An external stimulus (like a strain or temperature change) causes temporal and spectral shifts in the local Rayleigh backscatter pattern. These temporal and spectral shifts can be measured and scaled to give a distributed temperature or strain measurement [21]. More information on the system characteristics is available in [13, 14]. This process is shown in Figure 13.
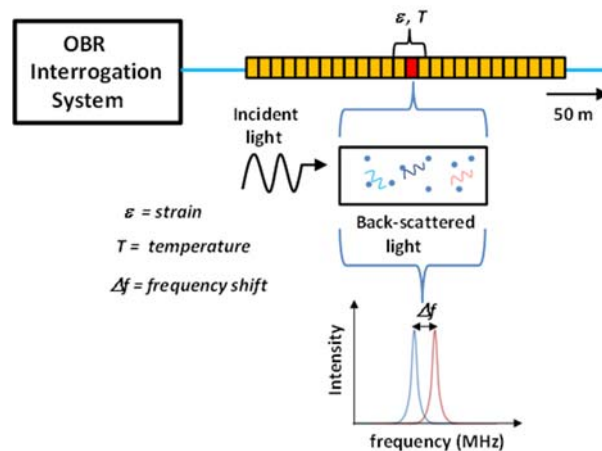
Figure 13. OBR measurement process [11].

Continuous strain data with high spatial resolution and ~~great~~ accuracy are the main advantages of OBR. This structural monitoring technique enables distributed strain measurements with millimetre-spatial resolution. Several experiences have demonstrated the feasibility of using this technique ~~either~~ in the structural monitoring of laboratory test [12] and existing concrete structures as well [16].

Several experiences have demonstrated the feasibility of using this technique either in the structural monitoring of existing concrete structures and in laboratory tests, both in bending and shear [16, 22, 23, 24]. In the specific case of detection and control of cracking in concrete structures, OBR system is an attractive monitoring tool.

Results and discussion

Using a coordinate system (x_n, y_n), as previously described, the location of appearing cracks was obtained. Thanks to 1 cm OBR system spatial resolution, the strain variation in the DOFS mesh of the tested beams could be obtained. In this way, both strain profiles in horizontal and vertical directions were measured simultaneously. In the right side of Figs 12 to 15, the horizontal strain evolution in the three tested beams versus different load levels from 100 to 262 kN is shown. Vertical strain evolution from 100 to 260 kN load level are shown in Figs 16 and 17. Localization, identification and progression of one or more cracks is represented using a 2D mesh and bold points at the left side of the figures. These bold points are identified with a letter and one number that represent the cracking location in 2D mesh section and the order how the cracking points appear. During the tests and to establish the order of appearance of the cracks, the sampling rate of the OBR system was 5s along the DOFS length. Once the crack points have been detected and located, it is also possible to obtain the strain values in the web for increasing load levels as presented in the Tables 3 to 6 for loads from 100 to 262 kN respectively. Additional information is available in [14].

Shear crack pattern

Through the analysis of the information obtained with the OBR system, the tracing of different cracking patterns in the 2D DOFS mesh area was achieved progressively as load was increasing. The shear crack patterns in the beams obtained with the DOFS strain data were validated thanks to the visual inspection carried out and photos taken during the test execution. More information about crack pattern recognition is available in [14, 24].

Shear crack angle

As explained in the theoretical background section of this paper, a key element needed to calculate the crack width is the angle of inclination of the shear crack. In this sense, the trace of shear cracking pattern also allows the calculation of the shear crack angles in two different ways. First, these angles can be obtained in detail with respect to the horizontal beam axis and with the point coordinates that define the beginning and end of the crack. Also global angles for the whole crack can be calculated using the average of the angle at different points of the crack. Shear crack patterns for each tested beam at 262, 260 and 258 kN are shown from Figs. 18 to 20. Shear crack angles at several points and the mean values for the global crack are shown from Tables 9 to 11.

Table 3. Strain values in the cracking points in horizontal sections of the beam I-2

Section	Load (kN) Cracking point	100 OBRmax με	142 OBRmax με	260 OBRmax με
A	A1		3045	12182
	A2			18077
	A4			1483
	A5			1483
	A3			8689
B	B8			63
	B1	577	7626	12724
	B2		4735	842
	B3		5511	12724
	B4			4410
	B5			7632
	B6			8324
	B7			4372
	B9			460
	B10			3055
	B11			343
C	C1	7815	5697	7105
	C9			3576
	C2	7178	1392	2897
	C3	412	4682	2897
	C4		12620	3237
	C5		1732	9752
	C6			3576
	C7			3848
	C8			3848
	C10			8667
	C11			5952
	C12			3848
D	D1	8261	693	14723
	D5		686	1472
	D2	1916	15335	4246
	D3	1187	1660	10115
	D4		2011	13482
	D6		3902	8894
	D8			13664
	D7			10775
	D9			7576
	D10			6668
	D11			12300

Table 4. Strain values in the cracking points in vertical sections of the beam I-2

Section	Load (kN) Cracking point	142 OBRmax με	260 OBRmax με
1	12		3791
	11		1675
	13		6492
2	21		21334
	22		13413
	23		8778
3	35		13821
	32		5508
	34		2333
	33		10438
	31		1957
	36		8599
4	43		12588
	41		3753
	42		7601
	44		17737
	45		4945
	46		9661
5	52		12966
	51		5635
6	62		6663
	61	869	17345
	63		145
	64		4977
7	74		12211
	73		4865
	71	2232	2332
	72		15631
8	84		4832
	83		1251
	81	3592	6593
	82		17008
	85		3060
	86		3347
9	91	14231	14114
	92		6856
	93		5469
	94		1229
	95		3920
10	101		1383
	102		2957
	103		11016
	104		2188
	105		9466

Table 5. Strain values in the cracking points in horizontal sections of the beam I-3

Section	Load (kN) Cracking point	158 OBRmax με	207 OBRmax με	258 OBRmax με
A	A1			4295
B	B3			6524
	B1		4086	7286
	B2			
	B4			3524
C	C2		2698	7250
	C1		3522	4871
	C4			12800
	C3			
	C5			6457
	C6			467
D	D1	409	11316	8467
	D2		2711	13701
	D3		2334	336
	D4		10760	4075
	D6			3981
	D7			897
	D8			2206
	D10			2486

Table 6. Strain values in the cracking points in vertical sections of the beam I-3

| Section	Load (kN) Cracking point	158 OBRmax με	207 OBRmax με	258 OBRmax με
3	31			542
4	42			429
	41			429
	43			6957
5	51			446
	52			502
	53			5432
	55			408
6	61		320	4886
	62		320	688
	63			565
	64			2786
	65			521
7	71		307	382
	72		384	5490
	73			382
	74			3379
	75			572
	76			509
8	81		379	15547
	83		358	3216
	84		253	6163
	82		2726	3669
	85			7613
	86			12192
	87			
9	91		3872	3420
	92		17940	4415
	93		1982	4372
	94		250	12304
	95			11622
	96		355	679
	97		302	15092
10	104		133	2125
	101		1920	10503
	103		6160	11226
	102		6053	37917
	105		293	735
	106			12361
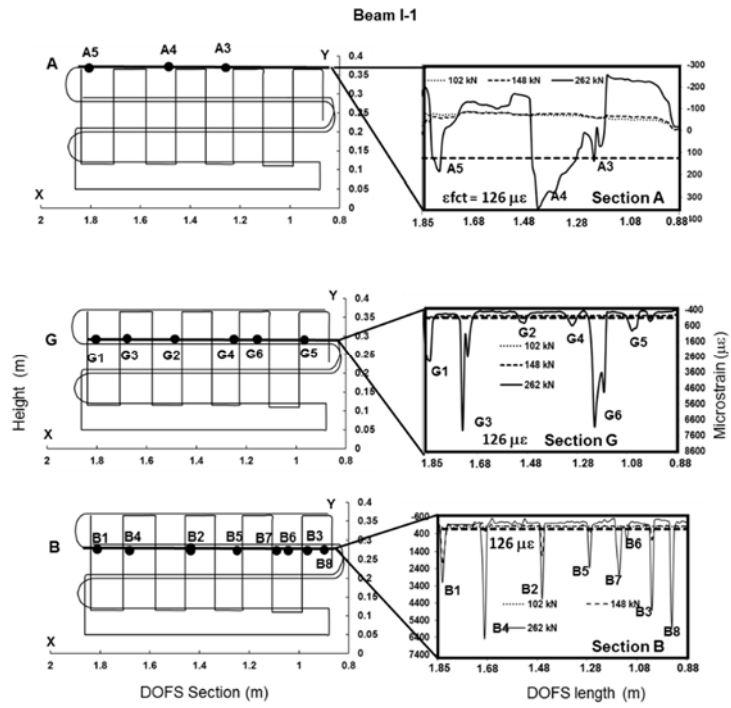
Fig. 12 Strain distribution and crack location in horizontal sections A, G and B of beam I-1 at different load level

Fig. 13 Strain distribution and crack location in horizontal sections F, C and D of beam I-1 at different load levels.

Fig. 14 Strain distribution and crack location in horizontal sections A, B, C and D of beam I-2 at different load levels.
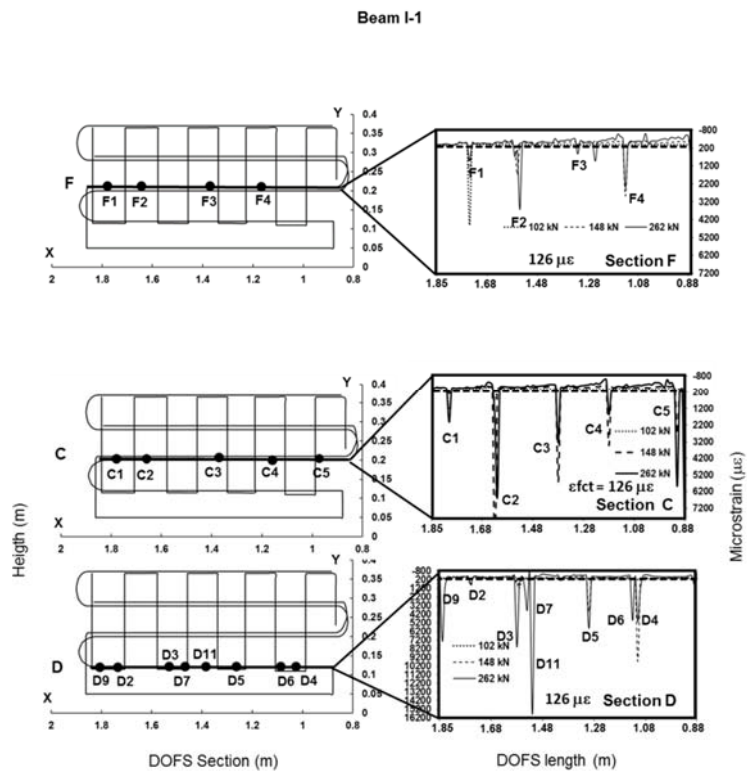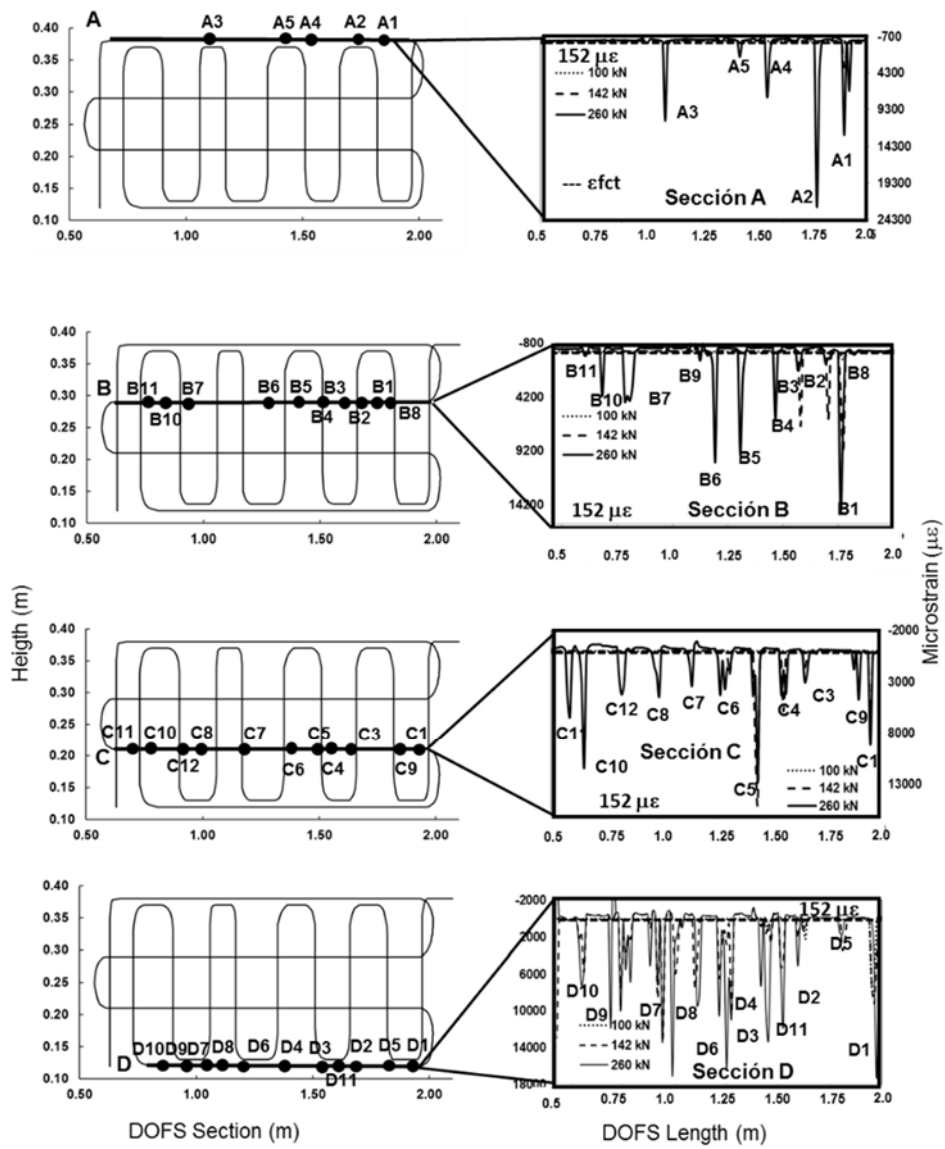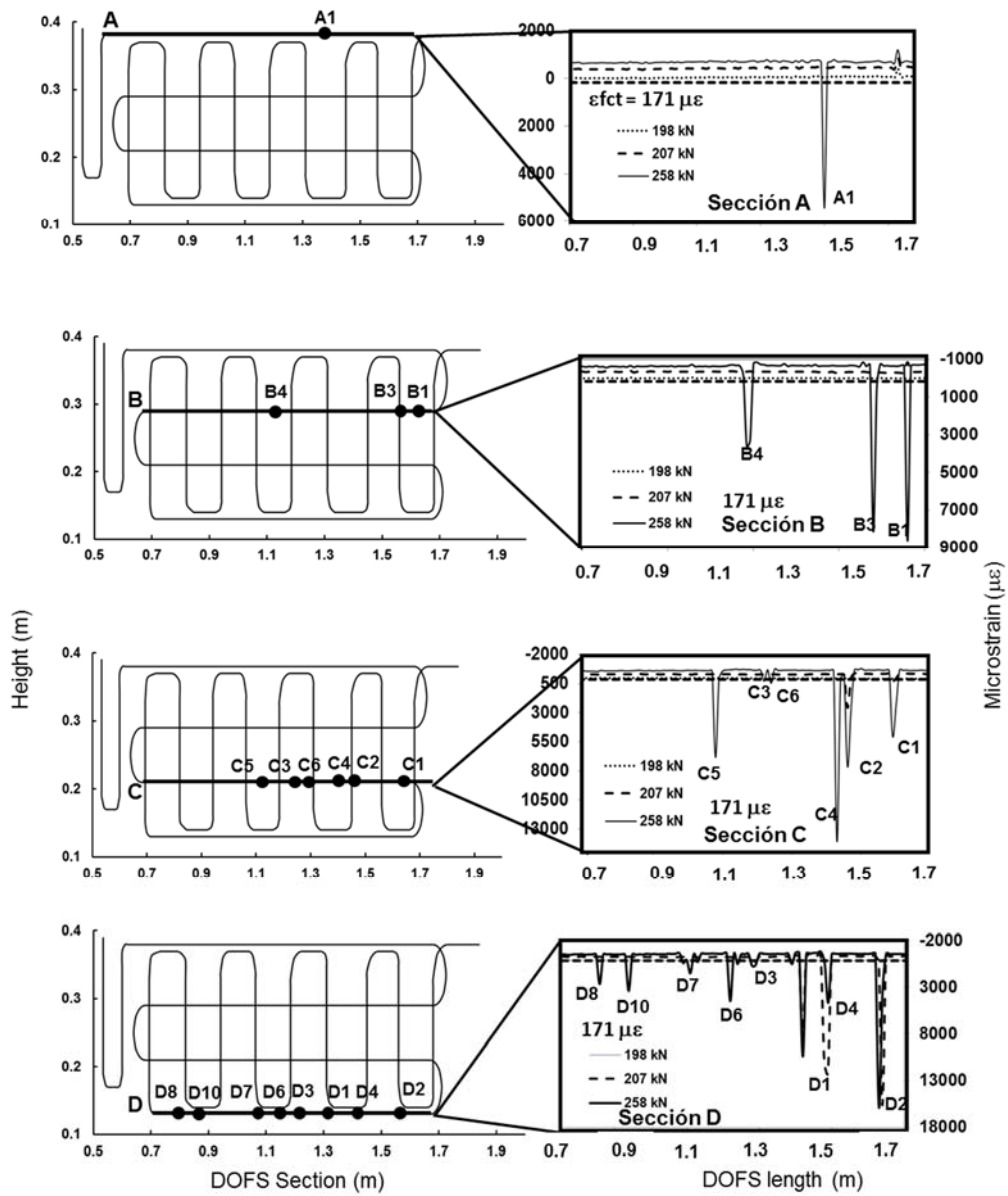
Beam I-3

Fig. 15 Strain distribution and crack location in horizontal sections A, B, C and D of beam I-3 at different load levels.
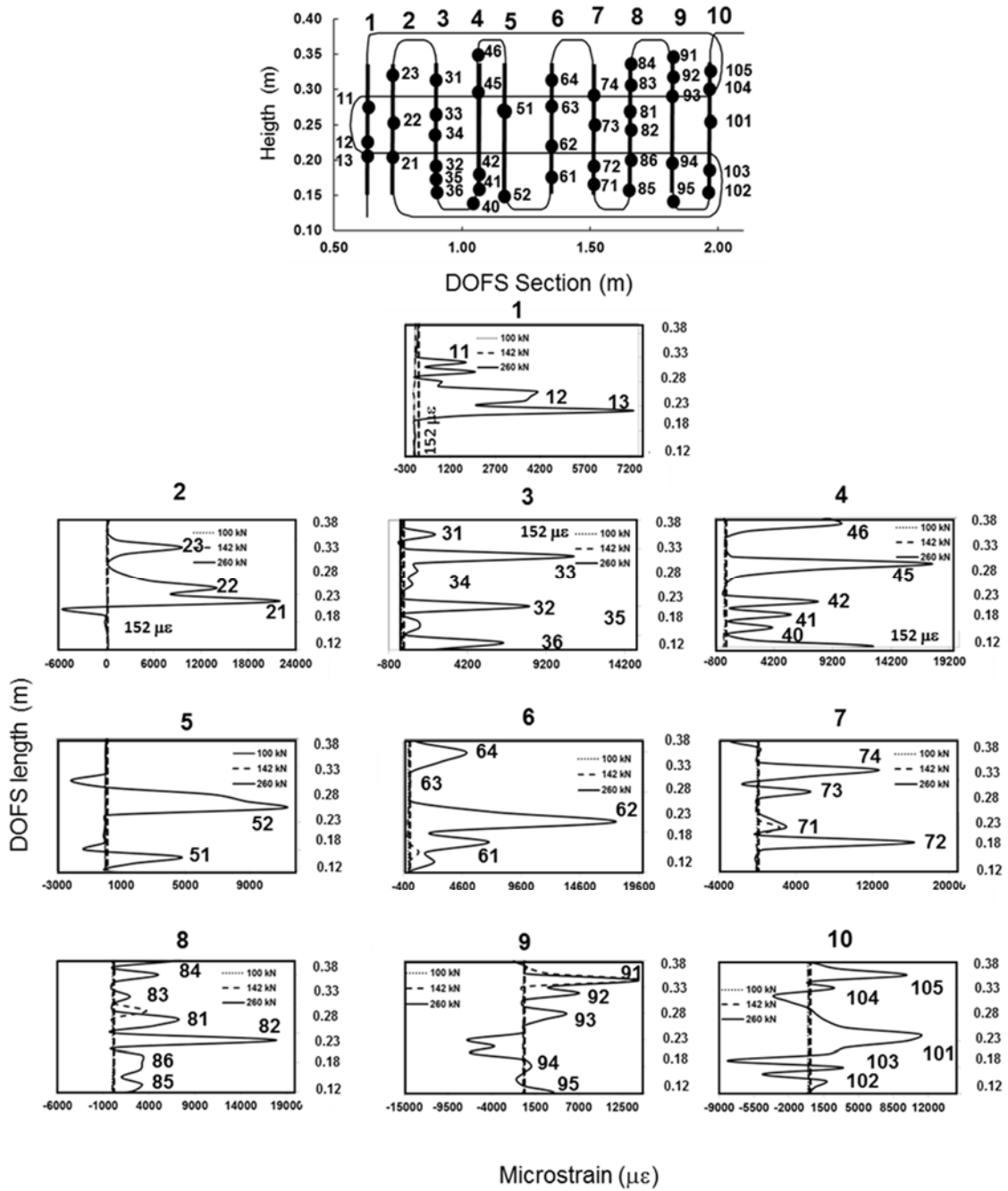
Beam I-2

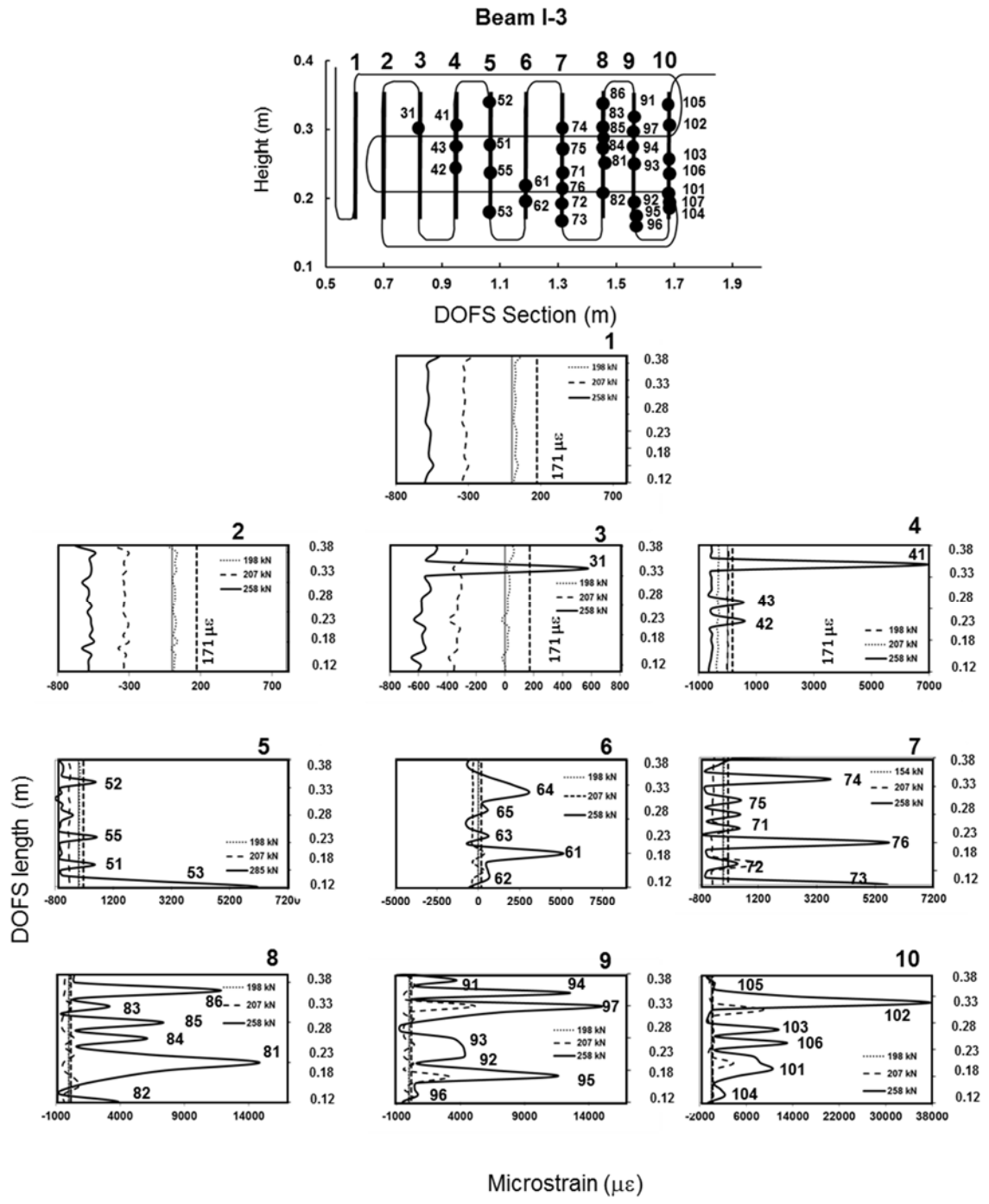Fig. 16. Strain distribution in vertical sections of beam I-2 at different load levels

Fig. 17. Strain distribution in vertical sections of beam I-3 at different load levels.
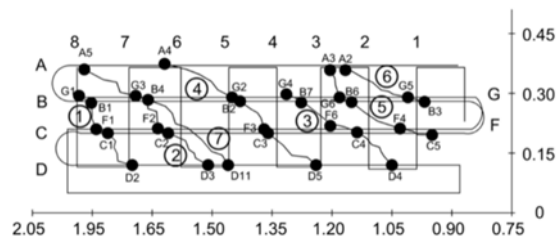

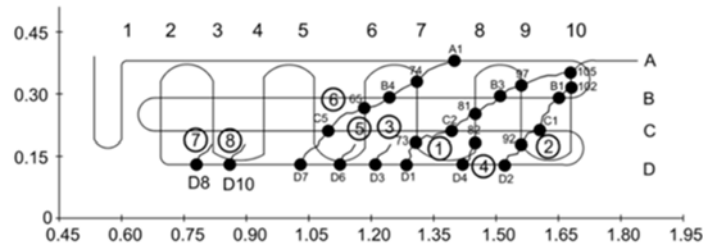Fig. 18. Shear crack pattern of beam I-1 at 262 kN.
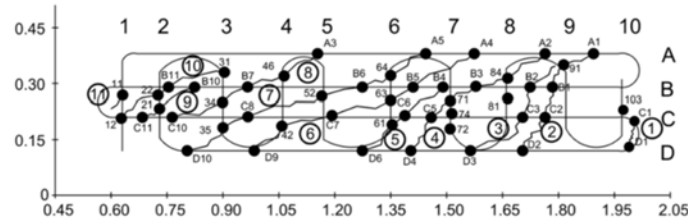
Fig. 19. Shear crack pattern of I-2 at 260 kN

Fig. 20. Shear cracking pattern of beam I-3 at 258 kN.

In Figs 18 to 20, total shear cracks are identified with a number and according to their order of appearance as deduced from the OBR strain data. This crack identification is shown in Tables 7 to 9. Different crack points that conform a total crack and its location respect to a coordinate system X-Y are also shown in these tables. Using some photos and crack drawings taken during the tests, curvilinear features between two consecutive points on a crack were traced in Figs. 18 to 20.

Shear crack width

Calculation of the average crack width was limited to the load level shown in Fig. 10. Up to this load level, the DOFS presented an acceptable behavior with very reliable results, which were confirmed with the crack widths obtained through the deformation rosettes. Therefore, continuous strain data obtained as shown in Figs. 12 to 17 were used to obtain the average crack width in each tested beam. The first step consisted in calculating the area under the curve of each strain profile from the tensile strain threshold (ε_{fct}) of each beam, and the distinction between the cracked length (Lcrack) and the effective lengths (Len) as shown in Fig. 3. This is done for x and y directions.

It must be noted that although the methodology proposed here can be used to obtain the crack width of any specific and single crack detected by the OBR system, in order to compare the results of the method with those of the rosettes, an average crack width in the whole cracked area is obtained. , This is just because the results from the rosettes represent the average values of cracking within the range of the rosette measurement indeed. In the case of beam I-1, the full experimental information of the DOFS was not available. Due to the failure in the DOFS2, the information of the vertical component of the shear strain was missing. Consequently, the results obtained from DOFS1, deployed in horizontal direction, are compared with those obtained by the horizontal components of the rosette only. Table 10 shows the average crack widths in the horizontal direction (wOBR) for each of the load levels studied in the case of beam I-1.

Table 7. Shear crack angles of beam I-1 at 262 kN.

Crack	Point	X	Y	Angle (°)
1	D2	1.7	0.12	45.0
	C1	1.78	0.2	45.0
	F1	1.79	0.21	66.8
	B1	1.82	0.28	45.0
	G1	1.83	0.29	Mean = 50.5
2	D3	1.51	0.12	38.7
	C2	1.61	0.2	45.0
	F2	1.62	0.21	66.8
	B4	1.65	0.28	26.6
	G3	1.67	0.29	Mean = 43.3
3	D4	1.05	0.12	36.0
	C4	1.16	0.2	4.1
	F6	1.3	0.21	21.3
	B7	1.12	0.28	4.1
	G4	1.26	0.29	Mean = 16.4
4	D5	1.24	0.12	33.7
	C3	1.36	0.2	45.0
	F3	1.37	0.21	49.4
	B2	1.43	0.28	26.6
	G2	1.45	0.29	25.0
	A4	1.3	0.36	Mean = 35.9
5	C5	0.89	0.2	2.0
	F4	1.17	0.21	41.2
	B6	1.09	0.28	9.5
	G6	1.15	0.29	47.1
	A3	1.215	0.36	Mean = 25
6	B3	0.99	0.28	26.6
	G5	1.01	0.29	20.7
	A2	1.195	0.36	Mean = 26.3
7	D11	1.46	0.12	40.1
	B4	1.65	0.28	26.6
	G3	1.67	0.29	25.0
	A5	1.82	0.36	Mean = 30.6

Table 8. Shear crack angles of beam I-2 at 260 kN.

Crack	Point	X	Y	Angle (º)
1	D1	1.99	0.13	82.6
	C1	2.00	0.20	45.7
	103	1.97	0.23	Mean = 60.1
2	D2	1.70	0.12	56.3
	C2	1.76	0.21	76.0
	B1	1.78	0.29	63.4
	91	1.81	0.35	20.6
	A1	1.89	0.38	Mean = 54.1
3	D3	1.56	0.12	32.7
	C3	1.70	0.21	51.3
	81	1.66	0.26	26.6
	B2	1.72	0.29	Mean = 36.9
4	D4	1.40	0.12	42.0
	C5	1.50	0.21	71.6
	71	1.51	0.24	26.6
	B3	1.61	0.29	60.9
	84	1.66	0.20	60.9
	A2	1.76	0.38	Mean = 52.4
5	D6	1.27	0.12	45.0
	61	1.35	0.20	14.0
	C6	1.39	0.21	33.7
	B4	1.51	0.29	Mean = 30.9
6	D9	0.98	0.12	51.3
	42	1.06	0.22	3.6
	C7	1.22	0.21	8.7
	63	1.35	0.19	73.3
	B5	1.38	0.29	28.3
	74	1.51	0.22	69.4
	A4	1.57	0.38	Mean = 41
7	D10	0.80	0.12	56.2
	35	0.90	0.27	19.4
	C8	1.07	0.21	21.8
	52	1.17	0.17	50.2
	B6	1.27	0.29	36.9
	64	1.35	0.23	59.0
	A5	1.44	0.38	Mean = 48.7
8	C10	0.76	0.21	32.7
	34	0.90	0.30	18.4
	B7	0.93	0.29	13.0
	46	1.06	0.32	33.7
	A3	1.15	0.38	Mean = 24.5
9	C11	0.71	0.21	56.3
	21	0.73	0.18	50.7
	B10	0.82	0.29	Mean = 43.8
10	12	0.63	0.17	11.3
	22	0.73	0.19	78.7
	B11	0.75	0.29	14.9
	31	0.90	0.33	Mean = 35
11	11	0.63	0.24	Mean = 45

Table 9. Shear crack angles of beam I-3 at 258 kN.

Crack	Point	X	Y	Angle (°)
1	D1	1.32	0.13	80.5
	73	1.31	0.19	8.7
	C2	1.44	0.21	44.6
	81	1.45	0.24	26.7
	B3	1.54	0.29	35.7
	97	1.56	0.21	31.2
	105	1.68	0.20	Mean = 33.4
2	D2	1.57	0.13	81.9
	92	1.56	0.20	26.6
	C1	1.58	0.21	58.0
	B1	1.63	0.29	11.3
	102	1.68	0.30	Mean = 44.4
3	D3	1.21	0.13	45.0
4	D4	1.42	0.13	80.0
	82	1.45	0.30	
5	D6	1.16	0.13	45.0
6	D7	1.03	0.13	16.3
	53	1.08	0.14	74.7
	C5	1.06	0.21	35.8
	65	1.19	0.30	15.9
	B4	1.15	0.29	39.9
	74	1.32	0.15	70.3
	A1	1.40	0.38	Mean =25.8
7	D8	0.78	0.13	45.0
8	D10	0.86	0.13	45.0

Table 10. Average crack width (wOBR) calculated for beam I-1 (102, 148 and 262 kN).

Load (kN)	102	148	262
Section	wOBR (mm)		
A			0.0090
G	0.0000	0.0144	0.0854
B	0.0001	0.0071	0.0441
Average	0.0000	0.0108	0.0462
F	0.0484	0.0126	0.0162
C	0.0058	0.0450	0.0430
D	0.0033	0.0268	0.0441
Average	0.0192	0.0281	0.0344

To compare average crack widths (wOBR) respect to the rosette data, only the horizontal potentiometers designated H3 and H1 were used on the top of the rosette, and the potentiometers H4 and H2 from the bottom. The above is indicated in Fig. 21. An average of potentiometers data H3 and H1, and potentiometers H4 and H2, were obtained and shown in Table 11. For a correct comparison, the DOFS horizontal sections were divided into two groups depending on their closeness to the corresponding potentiometers (see Fig. 21). First the readings of horizontal sections A, G and B (Fig.21) were considered and the average obtained was compared with the values of the wPoten Htop in Table 11.

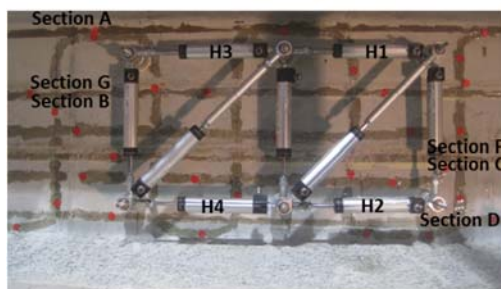Fig. 21. Horizontal potentiometers of beam I-1.

Table 11. Average shear crack width in the horizontal direction calculated for beam I-1

Load (kN)	*w*Poten Htop	wOBR (mm)	*w*Poten Hbottom	wOBR (mm)
102	-0.004	0.000	0.004	0.019
148	-0.006	0.011	0.037	0.028
262	0.066	0.046	0.037	0.034

The crack widths of horizontal sections F, C, and D were then averaged and compared with the values in the wPoten Hbottom column. Looking to Table 11, in general, the crack widths result with a good level of correspondence, especially at higher load levels. Results for other load levels than those shown in Table 13 are available in [6]. The average shear crack width for the beam I-2 was obtained using simultaneous strain data in two perpendicular directions X and Y. The areas under the curve were obtained both of the strain horizontal distribution of sections A, B, C and D (Fig. 4), and the vertical sections denominated 1 to 10 (Fig. 4). The obtained crack widths are shown in Table 12. The average shear crack widths obtained with the OBR method and the displacement values from the rosette placed in the web of beam I-2, are shown for comparison in Table 13. The diagonal potentiometers D1 and D2 shown in Fig. 22 were considered for comparison.

Table 12. Average shear crack width (wOBR) calculated for beam I-2

Load (kN)	100	142	260
Section	*w*OBR		
A		0.046	0.222
B	0.0072	0.092	0.148
C	0.1142	0.108	0.118
D	0.0588	0.069	0.254
Average	0.0601	0.079	0.185
10			0.223
9		0.188	0.112
8		0.039	0.130
7		0.025	0.135
6		0.008	0.149
5			0.331
4			0.275
3			0.122
2			0.207
1			0.107
Average		0.065	0.179

In general, the order of magnitude of the crack widths obtained in each type of instrumentation is similar, especially for the load levels in which the crack widths begin to be significant. It should be

taken into account that the comparison of results can only be done in an averaged way within the total cracked zone covered by the rosette´s displacements. Similar to the beam I-2, in the case of the I-3 beam, the wOBR crack widths were obtained, both for the horizontal and vertical sections of the DOFS. Table 14 shows the values and the average values for each section as well.
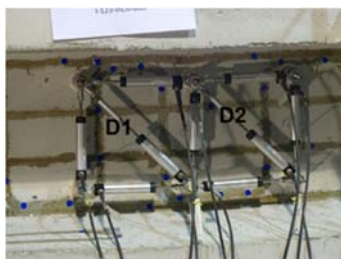

Fig. 22. Diagonal potentiometers of beam I-2

Table 13. Comparison of average crack widths D1, D2 and wOBRt for beam I-2

Load (kN)	D1_ponten (mm)	D2_ponten (mm)	*wOBRx* (mm)	*wOBRy* (mm)	*wOBRt* (mm)
100	0.023	0.000	0.060		0.060
142	0.038	0.048	0.079	0.065	0.102
260	0.337	0.345	0.185	0.179	0.258

Table 14. Average crack width (wOBR) calculated for beam I-3

Load (kN)	158	207	258
Section	*w*OBR (mm)		
A			0.0465
B		0.0127	0.0598
C		0.0147	0.0731
D	0.0023	0.0409	0.0546
Average	0.0023	0.0171	0.0585
10		0.0158	0.1967
9		0.0625	0.1104
8		0.0058	0.1105
7		0.0005	0.0161
6		0.0005	0.0242
5			0.0111
4			0.0244
3			0.0027
Average		0.0109	0.0619

It is observed that, unlike beam I-2, in which the first cracks were detected in horizontal sections, and only at higher load levels cracks appeared in the vertical sections, in beam I-3 cracks appear in both directions practically simultaneously.
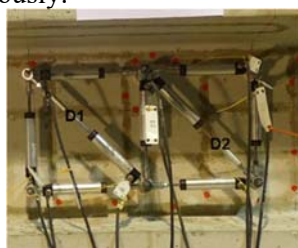

Fig. 23. Diagonal potentiometers of beam I-3.

In Table 15, the average crack widths obtained in each of the diagonal potentiometers (D1 and D2 in Fig. 23) are compared to those resulting from the crack widths (wOBR)

Table 15. Comparison of average crack widths D1, D2 and wOBRt for beam I-3

Carga (kN)	D1 (mm)	D2 (mm)	*wOBRx* (mm)	*wOBRy* (mm)	*wOBRt* (mm)
159	0.013	0.016	0.002	0.000	0.002
207	0.017	0.021	0.017	0.011	0.020
258	0.092	0.014	0.073	0.062	0.096

At a comparative level and in a general way, the order of the crack widths obtained in each type of instrumentation is similar. In this case, the crack widths obtained with potentiometer D1 (Fig. 23) and the resulting values wOBRt are very similar. In comparison to the crack widths obtained in the two previous beams, in the case of beam I-3, the measured crack widths are significantly lower. The above is explained by the higher shear resistance in beam I-3 compared to beams I-1 and I-2. In fact, in beam I-3 the first crack in the region subject to shear was detected at 158 kN, while in the other beams it was around 60 and 67 kN [14]. Also, when observing the cracking patterns of each beam, it can be seen that, for similar load levels, beam I-3 presents a lower cumulative damage level. We should bear in mind that beam I-3 has a web thickness 50 % higher than the other 2 beams.

Conclusions

Detection and localization of shear cracking using the DOFS and the OBR system presented an excellent performance. The detection in the initiation of the cracks in relation to the load level in each test could be made with a good precision. This allowed to obtain a shear crack pattern through the OBR system that could be visually contrasted with the cracking obtained in the tests, the correlation being also excellent.

Concerning the results obtained for the crack width, the proposed method and the most traditional method based on the deployment of displacement rosettes have provided similar results that are of the same order of magnitude, what validates the use of DOFS with the proposed OBR method to guess the average crack width under normal service loads. The matching between the results of the proposed method and those obtained with the standard instrumentation (displacement rosettes) is not perfect due to the high level of measurement error involved in the rosette method. In fact, the shear crack may not flow completely perpendicular to the displacement transducer and the shear zone involved in the measurement by the last is smaller than in the case of the DOFS. The extension of the zone involved in the measurement with the displacement rosettes makes only possible a comparison on the average crack width. This is one of the main drawbacks of the standard measurement technique by rosettes that can be avoided by the use of DOFS, where crack width can be obtained for every single shear crack.

During the tests, points were detected that were not necessarily part of the cracked patterns. These points can be from small cracks that at higher load levels will be part of the formation of other cracks, damage in the bonding of the fiber, presence of small cavities in the concrete surface, and effects caused by the high level of strain to which the optical fiber is subjected during this type of tests up to failure. Also, from a certain level of strain, some of the readings from the DOFS showed a randomly behaviour (spikes), with extremely high values alternating from tension to compression strains. This behaviour is completely unrealistic. Therefore, to clarify the above aspects, it will be advisable to carry out more detailed laboratory studies in this regard, where the most important variants that may influence the acquisition of reliable information through the DOFS and the OBR system can be simulated in a controlled manner. However, the level of load where these measurement anomalies appear is much higher than the normal in-service load of a concrete structure. This validates the technique here presented to in-service monitoring the crack width of concrete elements subject mainly to shear.

Huge amounts of data are produced by DOFS system applications. In this first experience, a semi-automatic algorithm was conformed to analyze, draw and calculate the mean shear crack width and helped by manual checkings.   The complete automation of the process to obtain the cracking

characteristics [25] is an important aspect and future objective to develop looking to the practical implementation of SHM of in-service structures.

Acknowledgments

References

[1] De Silva S., Mutsuyoshi H. and Witchukreangkrai E. (2008). Evaluation of Shear Crack Width in I-Shaped Prestressed Reinforced Concrete Beams. Journal of Advanced Concrete Technology. Vol. 6, No. 3, pp 443-458.

[2] Adebar P. (2001). Diagonal cracking and Diagonal Crack Control in Structural Concrete. ACI SP-204: Design and Construction. Practices to Mitigate Cracking, pp. 85-106.

[3] Stoerzel J. and Randal N. (2015), Monitoring shear induced degradation of reinforced and pretensioned concrete members. IABSE Conference. Structural Engineering: Providing Solutions to Glogal Challenges. Geneva, Switzerland.

[4] Zakaria M., Ueda T., Wu Z. and Meng L. (2009). Experimental Investigation on shear cracking behaviour in reinforced concrete beams with shear reinforcement. Journal of Advanced Concrete Technology. Vol. 7 No.1. ; pp 79-95.

[5] Wong L., Rathnayaka S., Chiu W.K. and Kodikara J. (2018). Utilising hydraulic transient excitation for fatigue crack monitoring of a cast iron pipeline using optical distributed sensing. Structural Control and Health Monitoring, Volume 25, Issue 4 January

[6] Wang X., Shi B., Wei G., Chen S., Zhu H and Wang T. (2017). Monitoring the behavior of segment joint in a shield tunnel using distributed optic fiber sensors. Structural Control and Health Monitoring, Volume 25, Issue 1 July.

[7] Song Z., Zhang D., Shi B., Chen S and Shen M. (2016). Integrated distributed fiber optic sensing technology-based structural monitoring of the pound lock. Structural Control and Health Monitoring, Volume 25, Issue 1 July. Volume 24, Issue 7 September.

[8] Barrias A., Casas J.R., and Villalba S. (2018). Embedded Distributed Optical Fiber Sensors in Reinforced Concrete Structures—A Case Study. Sensors 18(4), 980; https://doi.org/10.3390/s18040980

[9] Henault J.M., Quiertant S., Delepine-Lesoille J., Salin G., Taillade F. and Benzarti K. (2012). Quantitative strain measurement and crack detection in RC structures using a truly distributed fiber optic sensing system. Construction and Building Materials, 37 pp 916-923.

[10] Billon A., Henault J.M., Quiertant M., Taillade F., Khadour A., Martin R.P. and Benzarti, K. (2015). Qualification of distributed optical fiber sensor bonded to the surface of a concrete structure: Amethodology to obtain quantitative strain measurements. Smart Materials and Structures 24, 115001

[11] Rodríguez G., Casas J.R. and Villalba S. (2015), "Cracking assessment in concrete structures by distributed optical fiber", Smart Materials and Structures, 24, 035005

[12] Villalba S. and Casas J.R. (2013), "Application of optical fiber distributed sensing to health monitoring of concrete structures", Mechanical Systems and Signal Processing, 39; pp 441-451.

[13] Casas J.R., Villalba S. and Villalba V. (2014) "Management and safety of existing concrete structures via optical fiber distributed sensing". Chapter of the book "Maintenance and Safety of Aging Infrastructure". Dan M. Frangopol and Yiannis Tsompanakis, Editors. CRC Press. Taylor and Francis.

[14] Rodríguez G. (2017). Monitorización de estructuras de hormigón mediante sensores de fibra óptica distribuida. Ph D Thesis, Technical University of Catalonia, UPC, Barcelona (in Spanish).

[15] LUNA, (2017), Application Note, ODiSI Sensor installation guide, EN-FY1701 Revision A.

[16] Barrias A., Rodríguez G., Casas J.R.and Villalba S. (2018), Applications of distributed optical fiber sensors for the health monitoring of two real structures in Barcelona. Structure and Infrastructure Engineering, Vol. 14, N. 7, 967-985. DOI: 10.1080/15732479.2018.1438479

[17] Hoult N.A., Ekim O. y Regier R. (2014) "Damage/Deterioration for Steel Structures Using Distributed Fiber Optic Stress Sensors", ASCE Journal of Engineering Mechanics, October, 1-9

[18] Regier R. (2013). "Application of fiber optics on reinforced concrete structures to develop a structural health monitoring technique. Master thesis, Queen´s Univ., Kingston, ON, Canada.

[19] Gifford D.K., Sang A.K., Kreger S.T., and Foggatt M.E. (2010) "Strain measurements of fiber loop rosette using high spatial resolution Rayleigh scatter distributed sensing". Proceedings of Fourth European Workshop on Optical Fiber Sensors. SPIE Vol. 7653-765333-1.

[20] **Henault, J.M., Salin, G.,Moreau, G., Quiertant, M.,Taillade, F., Benzarti, K.,Delepine-lesoille, S (2012)**, Analysis of the strain transfer mechanism between a truly distributed optical fiber sensor and the surrounding medium, Concrete Repair, Rehabilitation and Retrofitting III, Edited by Pilate Moyo, CRC Press 2012, p. 266-267.

[21] **Samiec D. (2012)**, "Distributed fibre-optic temperature and strain measurement with extremely high spatial resolution", Photonik International, 1, 10-13.

[22] **Barrias A., Casas J.R., and Villalba S. (2018b),** Performance analysis of distributed optical fiber bonding adhesives to concrete. Proceedings of 9th International Conference on Bridge Maintenance, Safety and Management, IABMAS 2018, Melbourne, Australia

[23] **Barrias A., Casas J.R, and Villalba S. (2018c),** On the bonding performance of distributed optical fiber sensors (DOFS) in structural concrete. Proceedings of The Sixth International Symposium on Life-Cycle Civil Engineering, IALCCE 2018, Ghent, Belgium.

[24] **Rodríguez G., Casas J.R., Villalba S. and Barrias A. (2016)** "Monitoring of shear cracking in partially prestressed concrete beams by distributed optical fiber sensors", Proceedings of 8th International Conference on Bridge Mantenance, Safety and Management, IABMAS 2016, Iguazu, Brazil

[25] **Buchoud E., Henault J.-M., D'urso G., Girard A., Blairon S., Mars J.I., Vravie V. (2012)** Development of an automatic algorithm to analyse cracks evolution in a reinforced concrete structure from strain measurement by DOFS, Civil Structural Health Monitoring Workshop (CSHM-4), Berlin, Germany.